Live imaging of the Foreign Body Reaction (FBR) to suture implantation in zebrafish reveals how dampening inflammation can reduce fibrosis

Authors – David B. Gurevich[1*], Kathryn E. French[1,2*], John D. Collin[3], Stephen J. Cross[4], Paul Martin[1,5,6]

[1]School of Biochemistry, Biomedical Sciences Building, University Walk, University of Bristol, Bristol, BS8 1TD, United Kingdom
[2]Department Oral and Maxillofacial Surgery, University Hospitals Bristol, Lower Maudlin Street, Bristol BS1 2LY, UK
[3]Bristol Royal Infirmary, University Hospitals Bristol NHS Trust, Upper Maudlin Street, Bristol BS2 8HW, United Kingdom
[4]Wolfson Bioimaging Facility, Faculty of Biomedical Sciences, University Walk, University of Bristol, Bristol, BS8 1TD, UK
[5]School of Physiology, Pharmacology and Neuroscience, Biomedical Sciences Building, University Walk, University of Bristol, Bristol, BS8 1TD, United Kingdom
[6]School of Medicine, UHW Main Building, Heath Park, University of Cardiff, Cardiff, CF14 4XN, United Kingdom
[*]Joint first authors.

Abstract

Interactions between biological tissues and implantable biomaterials such as surgical sutures lead to a Foreign Body Response (FBR), which can result in fibrotic encapsulation, scarring and biomaterial rejection. To investigate the cell and tissue signalling events that underlie development of an FBR, we use live imaging of transgenic zebrafish reporter lines to observe how inflammation and angiogenesis differ between a healthy acute wound and an FBR. We see an expanding zone of inflammation extending back from suture margins; this correlates to an avascular zone, and subsequently to a defined fibrotic encapsulation zone. We observe macrophage fusion to generate foreign body giant cells adjacent to the suture and this together with the degree of scarring is dependent on the biocompatibility of the suture used: sutures that induced more inflammation resulted in increased zones of avascularity and fibrosis. By genetically or pharmacologically modifying the inflammatory response we were able to minimise the FBR and normalise the status of the tissue surrounding these sutures. This new model of FBR in adult zebrafish allows us, for the first time, to live image the process and to modulate it in ways that may lead us towards new strategies to ameliorate and circumvent FBR in humans.

Introduction

The surgical implantation of medical devices and biomaterials - from pacemakers to replacement hips to the sutures that close up a wound - has increased greatly over recent years as technologies advance and the population ages (Major et al, 2015). Once a material is implanted in host tissue, the interactions between the biomaterial and surrounding cells and matrix are critical in determining whether successful integration occurs. In ideal instances, biomaterial implantation results in an acute inflammatory response that drives a significant and necessary wound angiogenic response and subsequently limited fibrosis/scarring; this scenario largely recapitulates acute wound healing and leads to resolution of the repair response and successful biomaterial integration. Failure of biomaterial integration can be due to the exacerbation of the Foreign Body Response (FBR), where acute inflammation transitions to chronic inflammation which is generally

accompanied by foreign body giant cell formation and results in fibrous encapsulation (Anderson et al, 2008). This response limits the efficacy of implantable biomaterials, leading to rejection and negative health consequences that impact patient quality of life and cause a significant burden to the health service.

Most previous studies of FBR have been performed on mammalian models such as dogs and mice, largely using histology on fixed samples as an endpoint (Klopfleisch, 2016; Selvig et al, 1998), although more recent intravital studies of implanted plastic chambers in a mouse skin fold model have enabled a degree of dynamic imaging of collagen deposition during FBR using second harmonics (Dondossola et al, 2016). However, these studies are not optimal for high resolution investigations of the multifaceted and dynamic molecular conversations that occur between tissue and biomaterial, which is needed to understand how some materials integrate while others fail and undergo extensive FBR.

We have developed a genetically tractable and translucent model of the FBR that allows for transgenic fluorescent marking of various cells and tissues, enabling the real-time visualisation of immune cell-foreign body interaction over time in a non-invasive manner (Witherel et al, 2017). Aside from external fibrin clot formation, most steps of mammalian wound repair appear to be well conserved in zebrafish and have previously been extensively characterised (Gurevich et al, 2018; Mathias et al, 2009; Renshaw et al, 2006; Richardson et al, 2013); all the initial tissue interactions that are believed to contribute to the development of FBR are known to be present. By fluorescently labelling leukocytes, inflammatory markers and blood vessels, we are able to study the dynamic activities of cells in response to the implanted biomaterials, observing the interactions between these cells and the subsequent fibrotic encapsulation, and how these interactions can be modulated to reduce fibrosis and improve integration of biomaterials.

Results

The extent of non-resolving scar surrounding the foreign material varies according to suture type.

Fibrotic encapsulation of foreign bodies, including biomaterials, is a key component of FBR, and is critically important in determining how well a material is integrated into the surrounding tissue (Mikos et al, 1998; Ward, 2008). Previous investigations have shown that materials vary in their biocompatibility, with a consequent variation in degree of inflammatory response and the extent to which fibrosis is induced following implantation (Bryers et al, 2012). To investigate whether zebrafish tissue exhibits a similar, variable fibrotic response during FBR to that seen in mammalian tissues, we implanted either 8-0 non-resorbable monofilament nylon or resorbable braided vicryl sutures into flank tissue anterior to the base of the tail fin (Figure 1A, B). Control acute wounds were generated by 'pulling through' a vicryl suture at the same location (Figure 1B). It is already established that, unlike mammalian skin, acute wounds in adult zebrafish skin initially deposit scar collagen but this subsequently resolves (Richardson et al, 2013). Our Masson's trichrome histological staining indicates persistent scarring and fibrosis in FBR instances by our endpoint of 28 days post suture implantation (DPS), contrasting with the resolving scarring observed in acute wound repair (Figure 1C, D, and see (Richardson et al, 2013)). Importantly, the extent of the fibrotic area surrounding vicryl sutures was much larger than the response to nylon sutures ($0.3257mm^2$ compared to $0.0379mm^2$, Figure 1D), suggesting that zebrafish tissues react to these materials in similar ways to mammalian tissue.

All suture types drive an exaggerated and prolonged immune cell response, and the degree of scarring correlates with the extent of inflammatory response

We next utilized the translucency of the fish to visualise the dynamic interactions underlying the establishment of the FBR, imaging the same fish and following the same FBR over extended time periods without the interference of a viewing chamber or other implanted

intrusions. We performed high resolution live imaging following suture implantation into Tg(*mpx*:GFP); Tg(*mpeg*:mcherry) double transgenic zebrafish, which mark neutrophils and macrophages, respectively (Ellett et al, 2011; Renshaw et al, 2006). By imaging the same fish at specific time points across the observed 28 DPW or DPS, we were able to determine the differences in immune cell response to the two suture materials versus acute (pull through sutures) wounding, over time (Figure 2A). Previous studies examining FBR showed that the first immune cells to encounter the biomaterial are neutrophils (Selders et al, 2017), an observation supported by our results. In acute wounds, neutrophil and macrophage numbers peak at 4 DPW and 14 DPW, respectively, after which they resolve back to uninjured levels (Figure 2B). We see a similar pattern for nylon sutures, although some persistent immune cells remain in the vicinity of the suture at 28 DPS (Figure 2B). By contrast, we observe a large and persistent immune response up to 28 DPS in vicryl sutured fish, with many immune cells, particularly macrophages, maintaining close contact with the suture area (Figure 2A, B); this immune cell retention appears to correlate with the extensive fibrosis seen in response to this suture type (Figure 1C, D).

Close observation of suture associated macrophages at timepoints beyond 14 days post implantation indicates that some are considerably larger than standard macrophages (Figure 2F). This is suggestive of a phenomenon seen in models of mammalian FBR and TB granulomas, where macrophages converge and fuse, transforming into foreign body giant cells as a consequence of chronic inflammation (Davis et al, 2002; Sheikh et al, 2015; ten Harkel et al, 2016). To examine whether a similar response to chronic inflammation may be occurring in the zebrafish, we used a Tg(*mpeg*:mCherry); Tg(*mpeg*:nlsClover) double transgenic fish, enabling visualization of both cytoplasm and nuclei of macrophages (Figure 2C). We observed some multinucleated macrophages in close proximity to the suture beginning from 14 DPS, with larger numbers around vicryl sutures than adjacent to nylon sutures (Figure 2D, E). Together, these results indicate that zebrafish immune cells interact with foreign bodies in very similar ways to those observed in mammalian models, and that these interactions may be a key component in directing the extent of fibrotic encapsulation in response to implanted biomaterials.

Extent of fibrosis reflects immune cell dynamics within the suture-adjacent tissue.
Having observed the differences in fibrosis and inflammation, we next wondered whether the dynamics of leukocyte behavior in response to the suture might provide insight into the development of the FBR. Performing timelapse photomicroscopy on Tg(*mpeg*:mcherry) transgenic zebrafish revealed that, within unwounded tissues, macrophages are relatively sparse and static (data not shown). Following acute wounding, neutrophils and macrophages rapidly migrate to the wound site and interact freely and randomly with damaged tissue; by one post wounding they their migration is still rapid, but their directionality reduced (Figure 3A-C). By contrast, suture implantation led to an increase in immune cell directionality at early timepoints (heatmaps reveal how clumps of cells appear to have synchronized directionality), but a marked reduction in speed at later timepoints, such that macrophages appear 'paralysed' in the tissue adjacent to the suture, particularly in the case of vicryl sutures (Figure 3B, C). This suppression of cell movement extended further from the vicryl suture than for nylon sutures and correlates with the increased extent of fibrosis associated with these sutures (Figure 1D). These results suggest that the fibrotic tissue encapsulating the foreign body might influence the behaviour of local immune cells, or vice versa, and suggests a causal association between inflammation and localized fibrosis that we might test in our model.

Tissue inflammation is exacerbated by FBR and induces the formation of an avascular region.
An effective angiogenic response is pivotal for both wound healing (Eming et al, 2014) and biomaterial integration (Spiller et al, 2015). Our previous work has indicated that pro-inflammatory macrophages expressing tumour necrosis factor α (tnfα) are critical in driving

sprouting angiogenesis during tissue repair, but that macrophages must switch to an anti-inflammatory, *tnfα* negative state at later stages to enable appropriate subsequent vessel remodelling and regression (Gurevich et al, 2018). We have used our suture implantation model to observe the dynamic changes that occur with respect to both tissue inflammation and angiogenesis during a FBR. We combined the Tg(*tnfα*:GFP) transgenic line that marks pro-inflammatory cells with the Tg(*mpeg*:mCherry) macrophage marker line to reveal macrophages with pro-inflammatory or anti-inflammatory phenotypes. Acute (pull through suture) wounding of these fish reveals that wound *tnfα* expression is largely by macrophages and restricted to the close wound proximity (Figure 4A-C). This *tnfα* response is transient, peaking at 7 days and entirely resolved by 28 days post wounding (Figure 4A, B), as previously described for acute wounds (Gurevich et al, 2018; Hubner et al, 1996; MacLeod & Mansbridge, 2016). By contrast, both nylon and vicryl sutures provoke a significant level of *tnfα* expression in stromal cells also in the vicinity of the foreign body, and this was maintained throughout the observed 28 days (Figure 4B). The proportion of pro-inflammatory macrophages present around the suture site appeared to be increased relative to acute wounds in vicryl sutured scenarios at all timepoints post 7 DPS (Figure 4A, C). The overall *tnfα* response induced by vicryl sutures extends out to a much larger area compared to the nylon suture, and the extent of *tnfα* expression is closely correlated with the subsequent extent of fibrosis zone for these two suture types. These results suggest that part of the FBR is due to general tissue inflammation, and that this varies with respect to the nature of the implanted material.

To examine the angiogenic response to suture implantation, we utilised the Tg(*fli*:GFP) transgenic line that marks all blood vessels (Lawson & Weinstein, 2002). Acute wounds (pull through sutures) showed a robust revascularisation response, which was largely completed by 14 DPW (Figure 4D, E). By contrast, both suture types displayed a reduced capacity to establish blood vessels within close proximity of the implantation site, leading to an avascular zone around the suture (Figure 4D, E). This avascular zone differed for the two suture types: while nylon sutures appeared to largely re-establish vascular supply by 28 DPS, vicryl sutures exhibited a progressive increase in the avascular zone, extending out to 350µm from suture at 28 DPS. Intriguingly, the avascular area for each of the suture types correlated with their respective inflammatory zones (Figure 4A-C), and the subsequent extent of the fibrotic area encapsulating each suture type. Together, these results suggest a close association between the various contributors to FBR – inflammation, fibrosis and impaired angiogenesis – with the extent of each dependent on the type of implanted biomaterial.

Dampening the inflammatory response results in reduced fibrosis and improved revascularization.

Several studies have examined the relationship between extended, 'chronic' inflammation in the context of impaired healing and how this leads to progressive fibrosis (Morais et al, 2010). To test whether this correlation might be causal in FBR, we next attempted to modulate the inflammatory response to suture implants. Our first manipulation utilized the *csf1ra* mutant that has previously been shown to suppress the normal wound inflammatory response (Gurevich et al, 2018) in combination with Tg(*tnfα*:GFP); Tg(*mpeg*:mCherry) transgenic lines. The *csfr1a* mutant led to a "rescue" of the chronic inflammatory state, with reduced expression of *tnfα* by stromal cells in the tissue around both nylon and vicryl sutures which thus more closely resembles that of acute pull through wounds at all timepoints (Figure 5A, B). Furthermore, combining the *csf1ra* mutant with Tg(*fli*:GFP) revealed a rescue of the avascular zone defect also, with vessels growing considerably closer to the implanted suture (Figure 5C, D).

To complement this genetic approach we also suppressed inflammation in wild type fish by treatment with hydrocortisone (from 7 days to 28 days post suture implantation – Figure 6A),

similar to treatment regimes used in previous zebrafish studies (Hasegawa et al, 2017; Richardson et al, 2013). This inflammation dampening treatment resulted in a similar rescue of FBR and restoration of tissue repair and biomaterial integration to that seen in the *csf1ra* mutant scenario (Figure 6B-F). Together, these results identify generalised chronic tissue inflammation as a likely candidate for driving the FBR process and leading to failure of biomaterial integration, and suggest that dampening of tissue inflammation might be key to ameliorate these problems in a clinical setting.

Discussion

Our new model of the foreign body response to suture implantation in zebrafish has allowed us to observe the dynamic interplay of inflammation on cells and tissues including the vasculature and stromal cells that deposit collagen at the damage site. These studies imply a direct relationship between the extent of the inflammatory response and the degree of fibrotic encapsulation of a foreign body such as a suture and have several implications for the clinic.

A reciprocal relationship between inflammation, angiogenesis and scarring

Our previous work, as well as that of others, has characterized a dramatic angiogenic response at sites of acute tissue damage resulting in a transient increase in vessel density in the vicinity of the damage site to fuel increased metabolic requirements as the wound heals; these vessels subsequently regress, remodel and normalize back to that seen in uninjured tissue as the repair process finishes (Gurevich et al, 2018; Johnson & Wilgus, 2014). This tightly regulated wound angiogenic response is presumed to be critical because failed angiogenesis associates with chronic, non-healing wounds (Demidova-Rice et al, 2012; Nunan et al, 2014). Interestingly, our current study indicates that biomaterial implantation leads to an avascular zone, which correlates closely with the extent of tissue inflammation, and subsequently also with the zone of fibrotic encapsulation that occurs as part of FBR. This avascular zone has also been observed in response to implantation of other biomaterials such as biosensors, and is known to impair the integration and function of such devices (Morais et al, 2010). Indeed, revascularization post implantation is considered a key element in determining whether a biomaterial integrates or fails (Morais et al, 2010; Yu et al, 2009); in support of this, we observed that vicryl sutures, which trigger a more extensive avascular zone, were far more likely to be rejected from fish tails than nylon sutures (data not shown).

Avascular zones are not an entirely pathological phenomenon; cartilage is avascular, as is the zone beneath the developing epidermis of embryonic skin. Establishment of these avascular territories does not involve inflammation and is believed to be due to presence of avascular glycosaminoglycans such as Hyaluronic Acid (Feinberg & Beebe, 1983; Martin, 1990). A better understanding of which signals drive the avascular zone in the context of a FBR, and whether they are directly or indirectly released by inflammatory cells, may guide us towards ways for improving vascularity and better tissue integration with implanted biomaterials.

Modulating the inflammatory cells to regulate angiogenesis and fibrosis

We have previously demonstrated that pro-inflammatory macrophages that form the first wave of an acute inflammatory response following wounding upregulate vascular endothelial growth factor (VEGF) and are important in driving sprouting angiogenesis (Gurevich et al, 2018); it is also clear that these pro-inflammatory cells induce collagen deposition and fibrosis at repairing wound sites (Cash et al, 2014; Cash & Martin, 2016; Wynn & Barron, 2010). Our current study reveals that the most extensive angiogenesis and most suppressed fibrosis responses are present in contexts where stromal *tnfα* expression is inhibited while

still permitting a strong pro-inflammatory macrophage response, as occurs when sutures are implanted into a *csf1ra* mutant fish or those treated with hydrocortisone. It appears that this reduction of the general inflammation 'load' at the site of biomaterial implantation may be a critical factor in determining whether the biomaterial will integrate or undergo rejection via FBR, given the association between implant failure, extent of angiogenesis and fibrosis. Recent attempts to make biomaterials more biocompatible have focused on the simplistic goal of reducing inflammation (Kim et al, 2017; Zhang et al, 2014); our results suggest that the distinction between pro-inflammatory macrophages and pro-inflammatory stromal cells is an important one, and should guide the development of further innovations.

What role for giant cells in the FBR?

Foreign body giant cells (FBGCs) which are presumed to be formed by macrophage fusion, were first described in 1974 (Mariano & Spector, 1974) and are considered a characteristic component of the clinical response to implanted materials as well as some parasitic infections (Chambers, 1978; Davis et al, 2002). Indeed, activation and aggregation of distinct, specialized macrophages in response to persistent and antagonistic stimuli such as mycobacterium are now thought to be the key events driving the formation of granulomas seen in TB (McClean & Tobin, 2016; Ramakrishnan, 2012). Our study is the first to dynamically image these cells aggregating in high densities prior to FBGC formation. We note that FBGCs are more commonly seen in the vicinity of vicryl versus nylon sutures, suggesting that there may be a threshold level for both cell density and phenotypic state of inflammatory response before fusion will occur. Macrophages that come into direct contact with certain biomaterials are believed to undergo a process of 'frustrated phagocytosis', where the inability to engage with the material drives the fusion process; this leads to a subsequent decrease in phagocytic ability and a concomitant increase in free radical, enzyme and acid release to degrade implanted materials (Anderson et al, 2008). However, many questions remain concerning the precise triggers and mechanisms that underlie this fusion process, to activate FBGC formation. Our model presents a valuable opportunity for unraveling the dynamic nature of these fusion mechanisms, and insight into what the specific function of FBGCs may be.

Adult zebrafish as an important new *in vivo* model of FBR and clinical implications

This study represents the first time that the cell and tissue interactions underlying the FBR between biomaterial and surrounding tissue have been imaged dynamically, *in vivo* and non-invasively. The numerous similarities to mammalian FBR marks the zebrafish as a valuable model for increasing our understanding of the cellular and molecular basis for FBR in response to specific biomaterials. Our approach is particularly powerful as it allows the examination of several key processes and cell players – inflammation, formation of FBGCs, and the angiogenic response – in the same animal over time, permitting the specific tracking and dissection of dynamic cell:cell conversations. In addition, the imaging opportunities in zebrafish combined with its genetic tractability and amenability for chemical/pharmacological intervention, have allowed us to investigate how modulating inflammation in various ways may impact on tissue restoration during FBR and will allow for further screening and refining methods for alleviating FBR and improving biomaterial integration.

Figure Legends

Figure 1: Extent of foreign body fibrotic encapsulation is dependent on suture type. A) Schematic illustration of the zebrafish suture model, with scanning electron micrograph showing a suture in place. B) Representative images of zebrafish following suture pull through (white circle), nylon suture (red circle) or vicryl suture (red braided circle), 1 day post suturing (DPS) with insets to show suture detail. C) Masson's Trichrome stained transverse sections of pull through at 7 DPS, nylon or vicryl sutured fish at 28 DPS, to indicate extent of fibrosis. Sutures indicated with black asterisk, zone of scarring and fibrotic encapsulation indicated by black dotted line overlay. D) Quantification of total area of fibrotic encapsulation, measured from images in C). Statistical significance, as measured by two-tailed t-test, is P = 0.0003. Scale bars: A = 1mm, B = 1mm, C = 100μm.

Figure 2: Magnitude of immune response and numbers of foreign body giant cells are greater for vicryl versus nylon sutures. A) Schematic and representative images of Tg(*mpx*:GFP); Tg(*mpeg*:mCherry) double transgenic zebrafish immediately prior to and following suture pull through, nylon suture or vicryl suture, at indicated timepoints. B) Quantification of neutrophil and macrophage numbers in the vicinity of wound/suture, measured from images in A). C) Schematic of macrophage fusion as we observe in the vicinity of the suture, and representative image of Tg(*mpeg*:mCherry) transgenic adult zebrafish at 28 DPS, showing larger "fused" macrophages (arrowheads) adjacent to vicryl suture with more typically sized macrophages distant from the suture. D) Representative images of Tg(*mpeg*:mCherry); Tg(*mpeg*:nlsClover) double transgenic zebrafish at 28 DPS, showing that the larger macrophages adjacent to sutures are indeed multinucleated, compared to normal sized, single-nucleated macrophages at more distal sites (respective regions indicated by colour coded dotted lines). E) Quantification of images from D, showing average volume of macrophages adjacent to wound/suture for pull through, nylon and vicryl sutures. Statistical significance, as measured by one-way ANOVA, is P ≤ 0.0001. Significance values: *P ≤ 0.05, **P ≤ 0.001, ***P ≤ 0.0001. Data information: error bars indicate mean ± SD. Scale bars: A = 200μm, D = 200μm.

Figure 3: Immune cell motility and directionality within suture-adjacent tissues is affected by implanted material. A) Endpoints from 90 minute long representative timelapse movies of Tg(*mpeg*:mCherry) transgenic adult zebrafish at the indicated timepoints post pull through or suture implant, showing the tracks of macrophages as they respond to the wound/suture. Associated heatmaps report the directionality of local macrophages with respect to the suture. Red indicates increased level of directionality towards suture. B) Quantification of mean macrophage speed at 1 day and 28 days post implantation (from tracking data), indicating how motility is suppressed at later timepoints. Statistical significance, as measured by one-way ANOVA, is P = 0.0007. C) Quantification of directionality of macrophages at 1 and 28 days post implantation. Statistical significance, as measured by one-way ANOVA, is P = 0.0041. Significance values: *P ≤ 0.05, **P ≤ 0.001. Data information: error bars indicate mean ± SD. Scale bars: A = 200μm.

Figure 4: Extent of *tnfα* expression and size of avascular zone are also dependent on suture type. A) Representative images of Tg(*tnfα*:GFP); Tg(*mpeg*:mCherry) double transgenic zebrafish immediately prior to and following suture pull through, or implantation of nylon or vicryl suture, at indicated timepoints, showing macrophages (red), pro-inflammatory macrophages (yellow), and stromal cells expressing *tnfα* in the vicinity of the wound/suture zone (green). B) Quantification of total inflammatory area surrounding the wound/suture, measured from images in A). C) Quantification of proportion of *tnfα* positive, pro-inflammatory macrophages measured from images in A). D) Representative images of Tg(*fli*:GFP) transgenic zebrafish immediately prior to and following suture pull through, nylon suture or vicryl suture, to reveal angiogenic response at the indicated timepoints. E) Quantification of the extent of avascular zone immediately adjacent to wound/suture,

measured from images in D). Data information: error bars indicate mean ± SD. Scale bars: A = 200μm, D = 200μm.

Figure 5: Genetic immunosuppression results in decreased fibrotic encapsulation and reduced avascular zone. A) Representative images of *csf1ra* $^{-/-}$ Tg(*tnfα*:GFP); Tg(*mpeg*:mCherry) double transgenic adult zebrafish immediately prior to and following suture pull through, or implantation of nylon or vicryl suture, at indicated timepoints. B) Quantification of the altered inflammatory area surrounding the wound/suture, measured from images in A). C) Representative images of Tg(*fli*:GFP) transgenic adult zebrafish immediately prior to and following suture pull through, or implantation of nylon suture or vicryl suture, at indicated timepoints. D) Quantification of avascular zone immediately adjacent to wound/suture, measured from images in C). Data information: error bars indicate mean ± SD. Scale bars: A = 200μm, E = 200μm.

Figure 6: Pharmacological interventions that dampen the inflammatory response result in decreased fibrotic encapsulation, a reduced avascular zone and fewer foreign body giant cells. A) Diagram showing Hydrocortisone treatment protocol used to dampen inflammation during FBR (7-28 DPS). B) Representative images of Tg(*tnfα*:GFP); Tg(*mpeg*:mCherry), Tg(*fli*:GFP) and Masson's trichrome stained sections of suture tissue at the indicated timepoints following vicryl suture implantation and treatment with Hydrocortisone. C) Quantification of total inflammatory area surrounding the wound/suture, measured from images as in B). Statistical significance, as measured by two-tailed t-test, is $P \leq 0.0001$. D) Quantification of proportion of *tnfα* positive, pro-inflammatory macrophages surrounding the wound/suture, measured from images as in B). Statistical significance, as measured by two-tailed t-test, is $P = 0.0429$. E) Quantification of total area of fibrotic encapsulation, measured from images as in B). Statistical significance, as measured by two-tailed t-test, is $P \leq 0.0001$. F) Quantification of avascular zone immediately adjacent to wound/suture, measured from images as in B). Statistical significance, as measured by two-tailed t-test, is $P = 0.0008$. Data information: error bars indicate mean ± SD. Scale bars: B = 200μm.

Materials and Methods

Zebrafish strains and maintenance

All experiments were conducted with approval from the local ethical review committee at the University of Bristol and in accordance with the UK Home Office regulations (Guidance on the Operation of Animals, Scientific Procedures Act, 1986). Wild type and transgenic lines Tg(*fli1*:eGFP) [referred to as Tg(*fli*:GFP)](Lawson & Weinstein, 2002), Tg(*mpx*:GFP)(Renshaw et al, 2006), Tg(*mpeg1*:mCherry) [referred to as Tg(*mpeg*:mCherry)](Ellett et al, 2011), TgBAC(*tnfα*:GFP)[referred to as Tg(*tnfα*:GFP)](Marjoram et al, 2015) were maintained on TL wild type background, and staging and husbandry were performed as previously described (Westerfield, 1995). The mutant strain used was *csf1ra*^{j4e1} (Parichy et al, 2000), maintained on AB background or used in combination with transgenic lines as indicated. *csf1ra*^{j4e1} mutants were genotyped by visual inspection for absence of mature xanthophores as previously described (Parichy et al, 2000).

Suture implantation into adult zebrafish

Adult zebrafish suturing was performed as previously described (Witherel et al, 2017). Briefly, zebrafish were anesthetized in tank system water with 0.1mg/mL tricaine (ethyl 3-aminobenzoate methanesulfonate, Sigma Aldrich, Hamburg, Germany) and subsequently placed onto a foam surgical stand for surgery. Single interrupted sutures were implanted by placing a single loop through the tail, approx. 3mm anterior to the tailfin, using either nylon non-absorbable sutures (Polyamide, 8-0 monofilament, 3/8 tapered needle, S&T, Neuhausen, Switzerland) or vicryl, absorbable sutures (Polyglactin, 8-0 braided, 3/8 needle, Ethicon, Somerville, NJ, USA). Pull through control wounds were generated by implantation of a suture at the exact same anatomical location, which was immediately 'pulled through' and removed.

Imaging of adult zebrafish

For all imaging experiments, fish were initially anaesthetized in 0.3% Danieau's solution with 0.1mg/mL tricaine, and subsequently imbedded in a 10cm petri dish, using 1.5% w/v agarose added over the tail. Care was taken to keep agarose away from the gills. For timelapse imaging, fish were maintained in a lightly anaesthetized state at 0.05mg/mL tricaine throughout to allow continued breathing; fish that were no longer breathing by the end of movie acquisition were excluded from analysis. Gross anatomical images were generated on a Leica M205 FA system (Leica Microsystems). Confocal images and timelapse movies were generated on a Leica SP8 MP/CLSM system (Leica Microsystems).

Hydrocortisone treatment

For drug treatments, fish were treated with 275μM Hydrocortisone (Sigma Aldrich) dissolved in ethanol, as previously described (Richardson et al, 2013). 0.1% absolute ethanol was used for all treatments as well as vehicle control.

Masson's Trichrome staining

Harvested fish tails were immediately fixed in 4% PFA overnight at 4°C on a rocker, washed with PBS and then decalcified in 0.5M ethylenediaminetetraacetic acid (EDTA) (Sigma Aldrich, Hamburg, Germany) for seven days at 4°C on a rocker, replacing the EDTA solution on the third day. Samples were then stained for Masson's Trichrome, as previously described (Witherel et al, 2017).

Transmission Electron Microscopy

Tails were harvested at 28 DPS, fixed and processed as previously described (Nunan et al, 2015). Ultrathin (0.02 μm) sections were images on a Tecnai 12-FEI 120 kV BioTwin Spirit transmission electron microscope.

Image analysis and statistics

All image analysis was performed in ImageJ. Detection, tracking and spatial analysis of immune cells used the Modular Image Analysis automated workflow plugin for Fiji (Cross, 2018; Rueden et al, 2017; Schindelin et al, 2012). Sample motion due to tissue growth was corrected using translation-based registration via the SIFT Align plugin for Fiji (Lowe, 2004; Saalfeld, 2008) followed by B-spline unwarping using the BUnwarpJ plugin (Arganda-Carreras et al, 2006). Noise was removed using a 3D median filter and immune cells isolated from background using the Otsu threshold method with a constant user-defined offset (Otsu, 1979). The binarised image was refined using 2D hole filling and a 3D intensity-based watershed transform (Legland et al, 2016). Immune cells were identified in 3D as contiguous regions of pixels labelled as foreground using the MorphoLibJ plugin [8]. Immune cells were tracked between frames using the Munkres algorithm with scores based on object centroid separation (Munkres, 1957). Track spatial coordinates were used to calculate instantaneous velocity and track orientation in the XY-plane. A static reference point corresponding to the suture was manually-identified in each video. The angle between the instantaneous track orientation and this point was also measured (i.e. an angle of 0° corresponds to a cell moving directly towards the suture).

All statistical analysis was performed using Graphpad Prism. Data was confirmed to be normally distributed via d'Agostino-Pearson test or Shapiro-Wilk test prior to further comparisons. Student's t-test were used except in the case of comparisons involving more than two groups; in these instances, one-way ANOVA was performed for all comparisons, and a Bonferroni multiple comparison test was subsequently performed.

References

Anderson JM, Rodriguez A, Chang DT (2008) Foreign body reaction to biomaterials. Seminars in immunology 20: 86-100

Arganda-Carreras I, Sorzano COS, Marabini R, Carazo JM, Ortiz-de-Solorzano C, Kybic J (2006) Consistent and Elastic Registration of Histological Sections using Vector-Spline Regularization. CVAMIA: Computer Vision Approaches to Medical Image Analysis 85-95

Bryers JD, Giachelli CM, Ratner BD (2012) Engineering biomaterials to integrate and heal: the biocompatibility paradigm shifts. Biotechnology and bioengineering 109: 1898-1911

Cash JL, Bass MD, Campbell J, Barnes M, Kubes P, Martin P (2014) Resolution mediator chemerin15 reprograms the wound microenvironment to promote repair and reduce scarring. Current biology : CB 24: 1406-1414

Cash JL, Martin P (2016) Myeloid Cells in Cutaneous Wound Repair. Microbiology spectrum 4

Chambers TJ (1978) Multinucleate giant cells. The Journal of pathology 126: 125-148

Cross S (2018) Modular Image Analysis v0.7.17. Zenodo,: doi: 10.5281/zenodo. 1997259

Davis JM, Clay H, Lewis JL, Ghori N, Herbomel P, Ramakrishnan L (2002) Real-time visualization of mycobacterium-macrophage interactions leading to initiation of granuloma formation in zebrafish embryos. Immunity 17: 693-702

Demidova-Rice TN, Durham JT, Herman IM (2012) Wound Healing Angiogenesis: Innovations and Challenges in Acute and Chronic Wound Healing. Advances in wound care 1: 17-22

Dondossola E, Holzapfel BM, Alexander S, Filippini S, Hutmacher DW, Friedl P (2016) Examination of the foreign body response to biomaterials by nonlinear intravital microscopy. Nature biomedical engineering 1

Ellett F, Pase L, Hayman JW, Andrianopoulos A, Lieschke GJ (2011) mpeg1 promoter transgenes direct macrophage-lineage expression in zebrafish. Blood 117: e49-56

Eming SA, Martin P, Tomic-Canic M (2014) Wound repair and regeneration: mechanisms, signaling, and translation. Science translational medicine 6: 265sr266

Feinberg RN, Beebe DC (1983) Hyaluronate in vasculogenesis. Science 220: 1177-1179

Gurevich DB, Severn CE, Twomey C, Greenhough A, Cash J, Toye AM, Mellor H, Martin P (2018) Live imaging of wound angiogenesis reveals macrophage orchestrated vessel sprouting and regression. The EMBO journal 37

Hasegawa T, Hall CJ, Crosier PS, Abe G, Kawakami K, Kudo A, Kawakami A (2017) Transient inflammatory response mediated by interleukin-1beta is required for proper regeneration in zebrafish fin fold. eLife 6

Hubner G, Brauchle M, Smola H, Madlener M, Fassler R, Werner S (1996) Differential regulation of pro-inflammatory cytokines during wound healing in normal and glucocorticoid-treated mice. Cytokine 8: 548-556

Johnson KE, Wilgus TA (2014) Vascular Endothelial Growth Factor and Angiogenesis in the Regulation of Cutaneous Wound Repair. Advances in wound care 3: 647-661

Kim H, Kim BH, Huh BK, Yoo YC, Heo CY, Choy YB, Park JH (2017) Surgical suture releasing macrophage-targeted drug-loaded nanoparticles for an enhanced anti-inflammatory effect. Biomaterials science 5: 1670-1677

Klopfleisch R (2016) Macrophage reaction against biomaterials in the mouse model - Phenotypes, functions and markers. Acta biomaterialia 43: 3-13

Lawson ND, Weinstein BM (2002) In vivo imaging of embryonic vascular development using transgenic zebrafish. Developmental biology 248: 307-318

Legland D, Arganda-Carreras I, Andrey P (2016) MorphoLibJ: integrated library and plugins for mathematical morphology with ImageJ. Bioinformatics 32: 3532-3534

Lowe D (2004) Distinctive Image Features from Scale-Invariant Keypoints. International Journal of Computer Vision 60: 91-110

MacLeod AS, Mansbridge JN (2016) The Innate Immune System in Acute and Chronic Wounds. Advances in wound care 5: 65-78

Major MR, Wong VW, Nelson ER, Longaker MT, Gurtner GC (2015) The foreign body response: at the interface of surgery and bioengineering. Plastic and reconstructive surgery 135: 1489-1498

Mariano M, Spector WG (1974) The formation and properties of macrophage polykaryons (inflammatory giant cells). The Journal of pathology 113: 1-19

Marjoram L, Alvers A, Deerhake ME, Bagwell J, Mankiewicz J, Cocchiaro JL, Beerman RW, Willer J, Sumigray KD, Katsanis N, Tobin DM, Rawls JF, Goll MG, Bagnat M (2015) Epigenetic control of intestinal barrier function and inflammation in zebrafish. P Natl Acad Sci USA 112: 2770-2775

Martin P (1990) Tissue patterning in the developing mouse limb. The International journal of developmental biology 34: 323-336

Mathias JR, Dodd ME, Walters KB, Yoo SK, Ranheim EA, Huttenlocher A (2009) Characterization of zebrafish larval inflammatory macrophages. Developmental and comparative immunology 33: 1212-1217

McClean CM, Tobin DM (2016) Macrophage form, function, and phenotype in mycobacterial infection: lessons from tuberculosis and other diseases. Pathogens and disease 74

Mikos AG, McIntire LV, Anderson JM, Babensee JE (1998) Host response to tissue engineered devices. Advanced drug delivery reviews 33: 111-139

Morais JM, Papadimitrakopoulos F, Burgess DJ (2010) Biomaterials/tissue interactions: possible solutions to overcome foreign body response. The AAPS journal 12: 188-196

Munkres J (1957) Algorithms for the Assignment and Transportation Problems. Journal of the Society for Industrial and Applied Mathematics 5: 32-38

Nunan R, Campbell J, Mori R, Pitulescu ME, Jiang WG, Harding KG, Adams RH, Nobes CD, Martin P (2015) Ephrin-Bs Drive Junctional Downregulation and Actin Stress Fiber Disassembly to Enable Wound Re-epithelialization. Cell reports 13: 1380-1395

Nunan R, Harding KG, Martin P (2014) Clinical challenges of chronic wounds: searching for an optimal animal model to recapitulate their complexity. Dis Model Mech 7: 1205-1213

Otsu N (1979) A threshold selection method from gray-level histograms. IEEE Trans Sys, Man, Cyber 9: 62-66

Parichy DM, Ransom DG, Paw B, Zon LI, Johnson SL (2000) An orthologue of the kit-related gene fms is required for development of neural crest-derived xanthophores and a subpopulation of adult melanocytes in the zebrafish, Danio rerio. Development 127: 3031-3044

Ramakrishnan L (2012) Revisiting the role of the granuloma in tuberculosis. Nature reviews Immunology 12: 352-366

Renshaw SA, Loynes CA, Trushell DM, Elworthy S, Ingham PW, Whyte MK (2006) A transgenic zebrafish model of neutrophilic inflammation. Blood 108: 3976-3978

Richardson R, Slanchev K, Kraus C, Knyphausen P, Eming S, Hammerschmidt M (2013) Adult zebrafish as a model system for cutaneous wound-healing research. The Journal of investigative dermatology 133: 1655-1665

Rueden CT, Schindelin J, Hiner MC, DeZonia BE, Walter AE, Arena ET, Eliceiri KW (2017) ImageJ2: ImageJ for the next generation of scientific image data. BMC bioinformatics 18: 529

Saalfeld S (2008) Linear Stack Alignment with SIFT v1.2.0. plugin for Fiji https://github.com/axtimwalde/mpicbg

Schindelin J, Arganda-Carreras I, Frise E, Kaynig V, Longair M, Pietzsch T, Preibisch S, Rueden C, Saalfeld S, Schmid B, Tinevez JY, White DJ, Hartenstein V, Eliceiri K, Tomancak P, Cardona A (2012) Fiji: an open-source platform for biological-image analysis. Nature methods 9: 676-682

Selders GS, Fetz AE, Radic MZ, Bowlin GL (2017) An overview of the role of neutrophils in innate immunity, inflammation and host-biomaterial integration. Regenerative biomaterials 4: 55-68

Selvig KA, Biagiotti GR, Leknes KN, Wikesjo UM (1998) Oral tissue reactions to suture materials. The International journal of periodontics & restorative dentistry 18: 474-487

Sheikh Z, Brooks PJ, Barzilay O, Fine N, Glogauer M (2015) Macrophages, Foreign Body Giant Cells and Their Response to Implantable Biomaterials. Materials 8: 5671-5701

Spiller KL, Freytes DO, Vunjak-Novakovic G (2015) Macrophages modulate engineered human tissues for enhanced vascularization and healing. Annals of biomedical engineering 43: 616-627

ten Harkel B, Koopsen J, van Putten SM, van Veen H, Picavet DI, de Vries TJ, Bank RA, Everts V (2016) Ultrastructural aspects of foreign body giant cells generated on different substrates. Journal of structural biology 195: 31-40

Ward K (2008) A review of the foreign-body response to subcutaneously-implanted devices: the role of macrophages and cytokines in biofouling and fibrosis. Journal of diabetes science and technology 2: 768-777

Westerfield M (1995) The Zebrafish Book. A Guide for the Laboratory Use of Zebrafish (Danio rerio), 3rd Edition., Eugene, OR: University of Oregen Press.

Witherel CE, Gurevich DB, Collin JD, Martin P, Spiller KL (2017) Host-biomaterial Interactions in Zebrafish. ACS Biomater Sci Eng 14: 1-8

Wynn TA, Barron L (2010) Macrophages: master regulators of inflammation and fibrosis. Seminars in liver disease 30: 245-257

Yu H, VandeVord PJ, Mao L, Matthew HW, Wooley PH, Yang SY (2009) Improved tissue-engineered bone regeneration by endothelial cell mediated vascularization. Biomaterials 30: 508-517

Zhang S, Liu X, Wang H, Peng J, Wong KK (2014) Silver nanoparticle-coated suture effectively reduces inflammation and improves mechanical strength at intestinal anastomosis in mice. Journal of pediatric surgery 49: 606-613

Figure 1

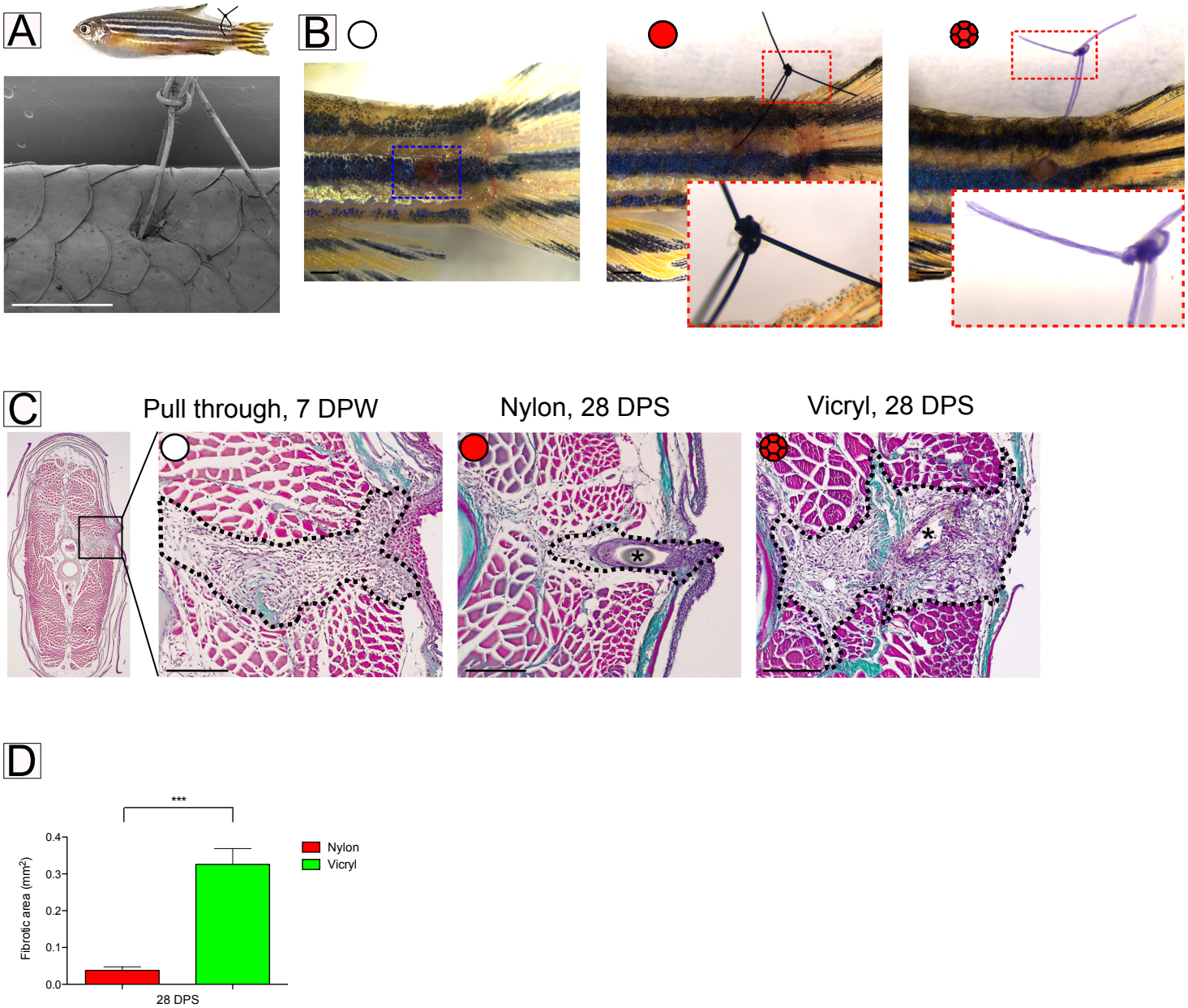
A
B
C
Pull through, 7 DPW
Nylon, 28 DPS
Vicryl, 28 DPS
D
***
Fibrotic area (mm²)
0.4
0.3
0.2
0.1
0.0
28 DPS
Nylon
Vicryl

Figure 2

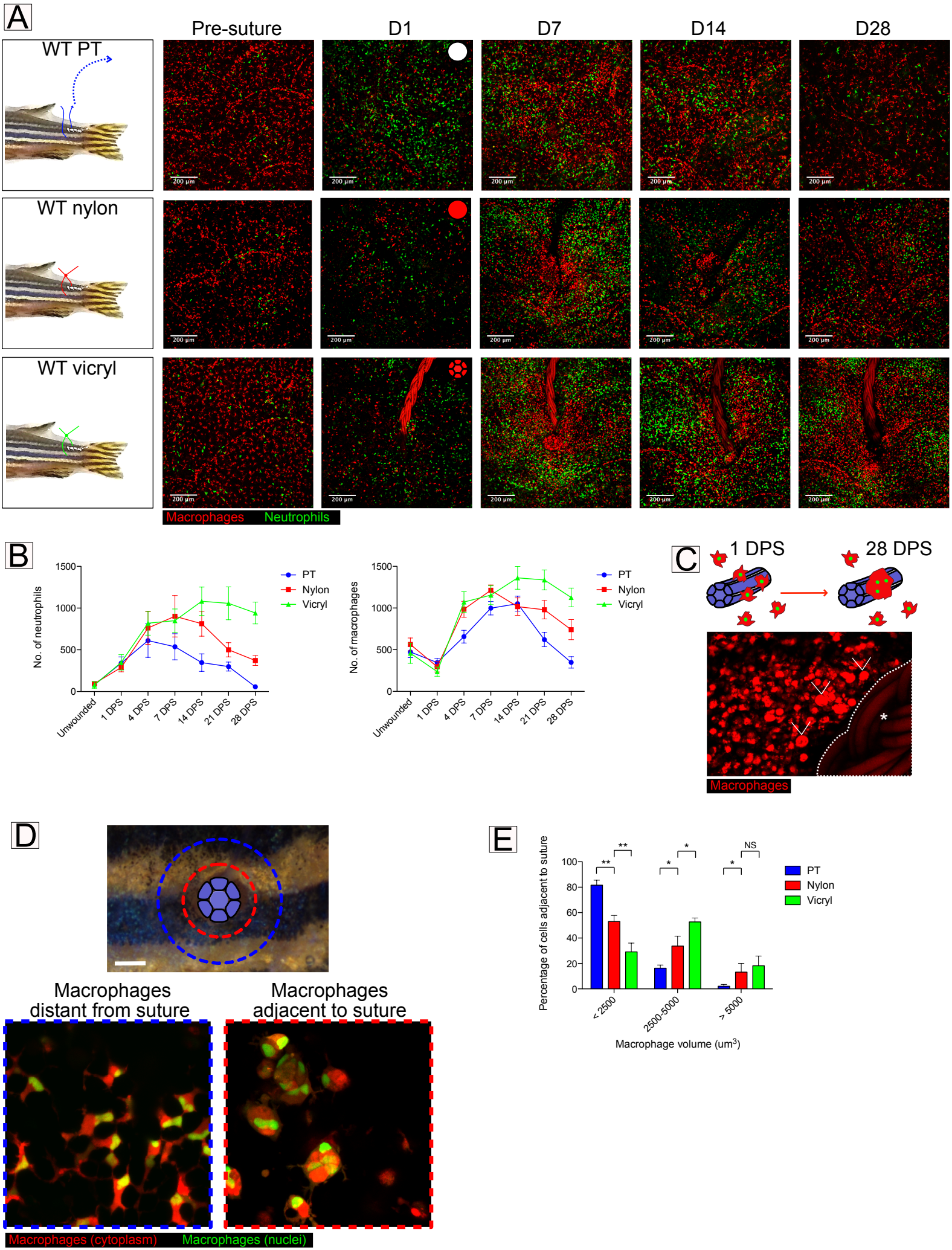
A
Pre-suture
D1
D7
D14
D28
WT PT
WT nylon
WT vicryl
200 µm
Macrophages
Neutrophils
B
No. of neutrophils
No. of macrophages
1500
1000
500
0
Unwounded
1 DPS
4 DPS
7 DPS
14 DPS
21 DPS
28 DPS
PT
Nylon
Vicryl
C
1 DPS
28 DPS
Macrophages
D
Macrophages distant from suture
Macrophages adjacent to suture
Macrophages (cytoplasm)
Macrophages (nuclei)
E
Percentage of cells adjacent to suture
100
80
60
40
20
0
**
*
NS
< 2500
2500-5000
> 5000
Macrophage volume (um3)
PT
Nylon
Vicryl

Figure 3

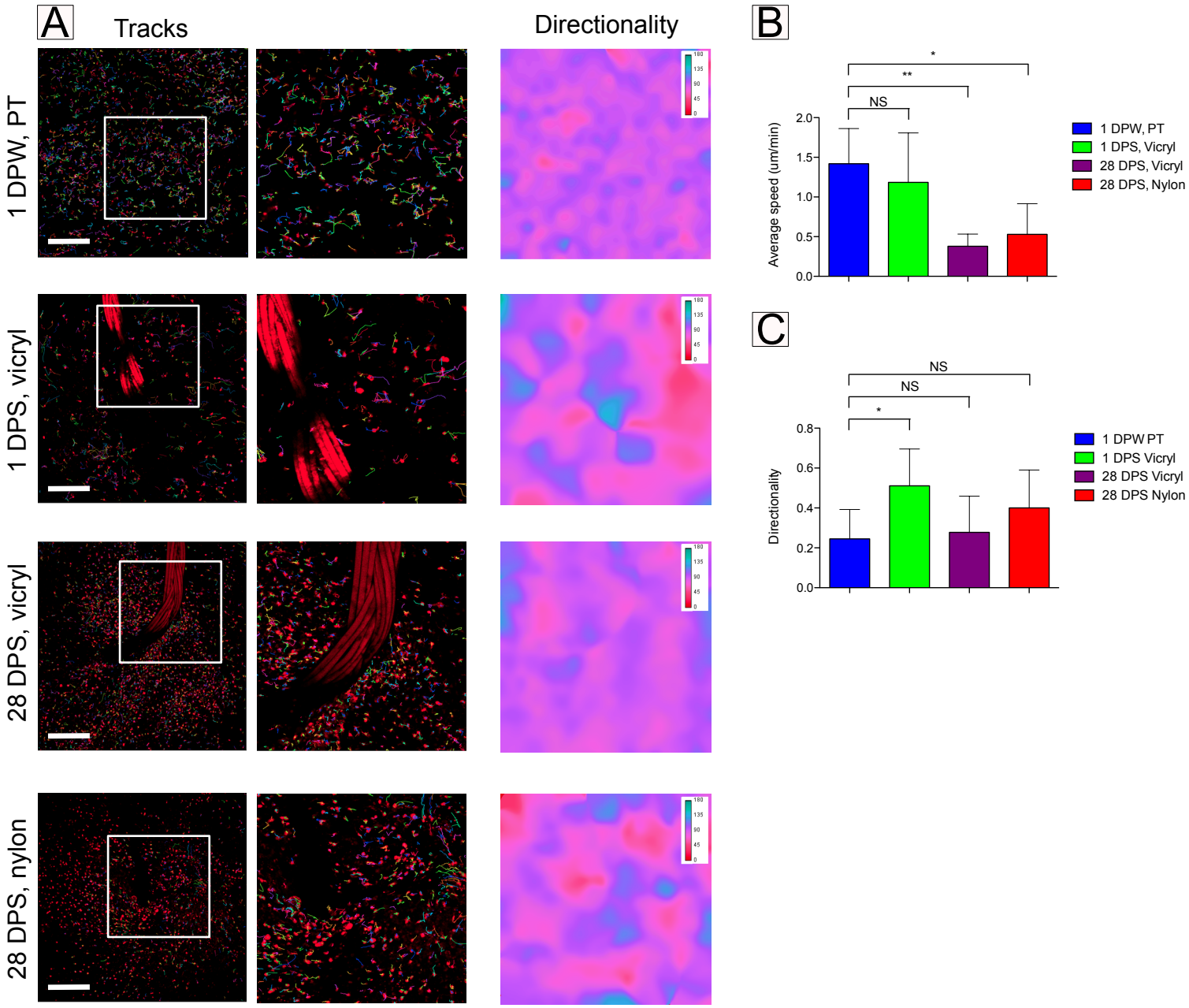
A
Tracks
Directionality
1 DPW, PT
1 DPS, vicryl
28 DPS, vicryl
28 DPS, nylon
B
Average speed (um/min)
2.0
1.5
1.0
0.5
0.0
NS
**
*
1 DPW, PT
1 DPS, Vicryl
28 DPS, Vicryl
28 DPS, Nylon
C
Directionality
0.8
0.6
0.4
0.2
0.0
NS
NS
*
1 DPW PT
1 DPS Vicryl
28 DPS Vicryl
28 DPS Nylon

Figure 4

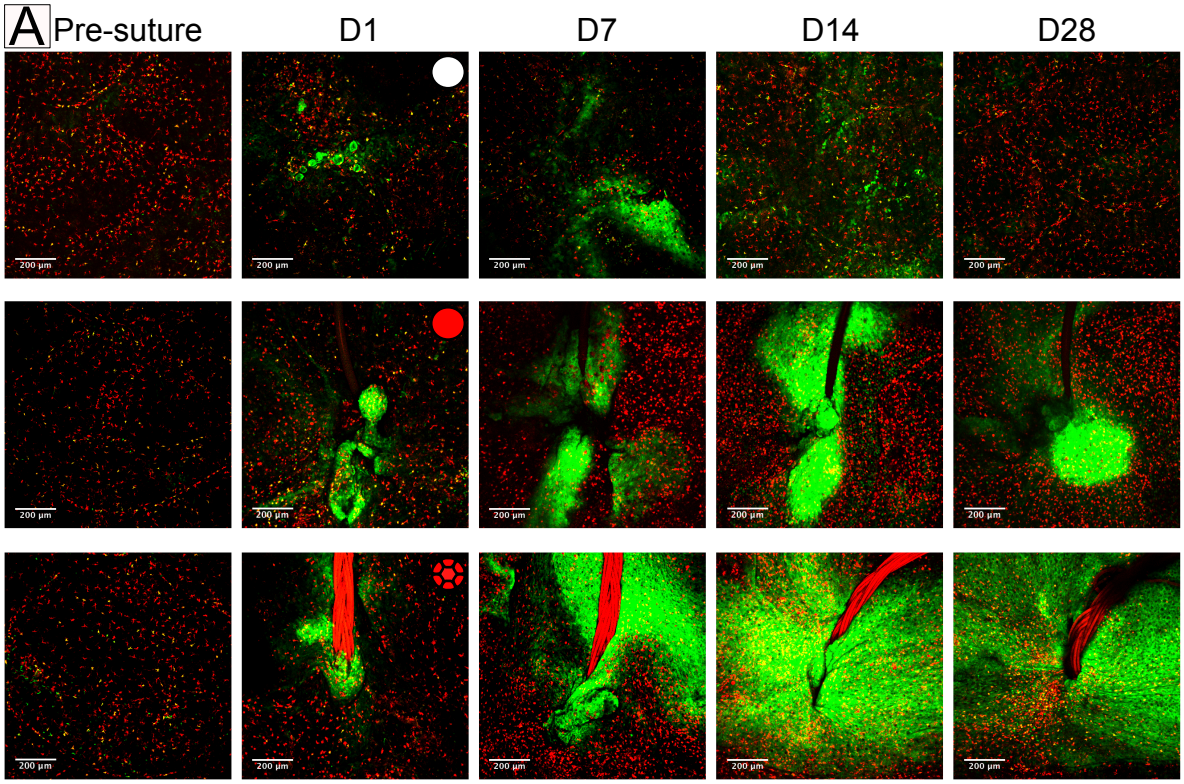
A
Pre-suture
D1
D7
D14
D28
200 µm
Macrophages
tnfα
tnfα+ve macrophages

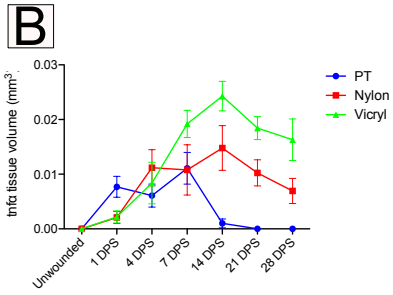
B
tnfα tissue volume (mm³)
0.03
0.02
0.01
0.00
Unwounded
1 DPS
4 DPS
7 DPS
14 DPS
21 DPS
28 DPS
PT
Nylon
Vicryl

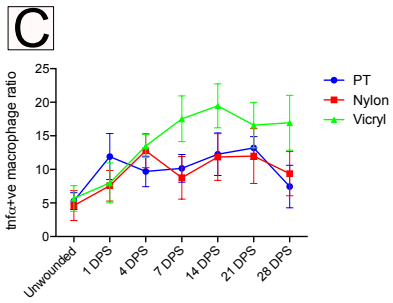
C
tnfα+ve macrophage ratio
25
20
15
10
5
0
Unwounded
1 DPS
4 DPS
7 DPS
14 DPS
21 DPS
28 DPS
PT
Nylon
Vicryl

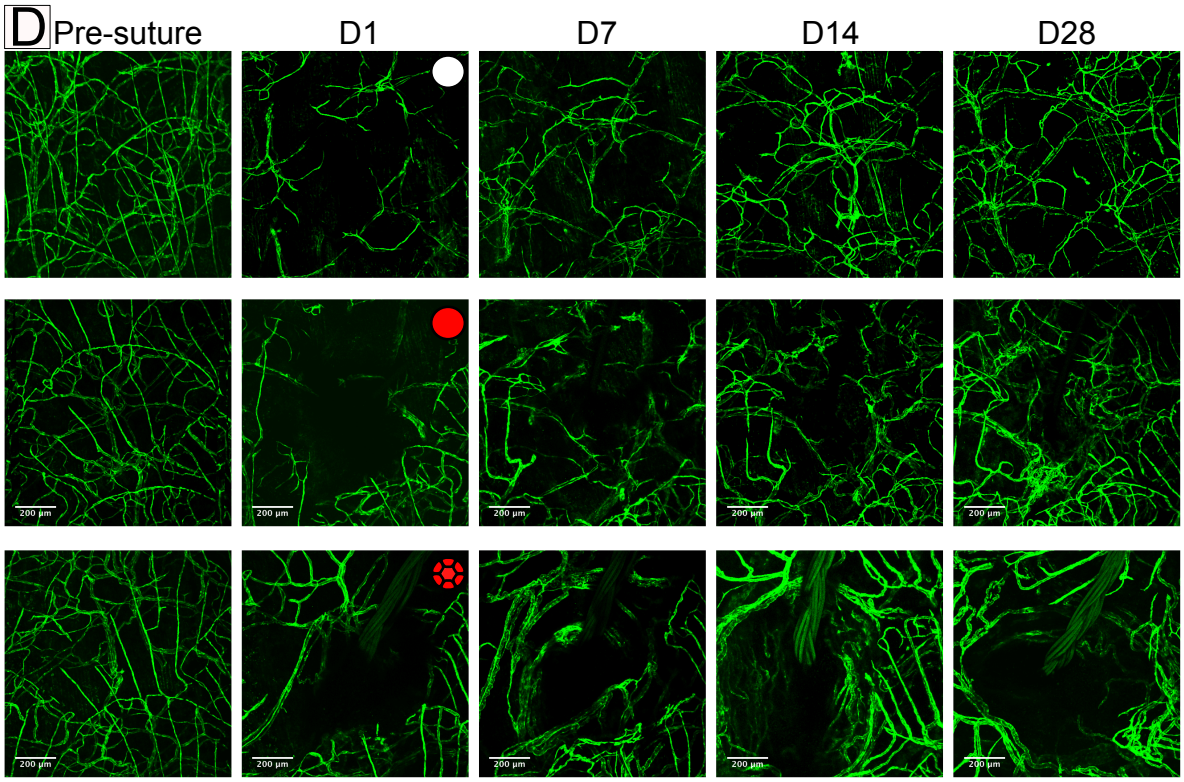
D
Pre-suture
D1
D7
D14
D28
200 µm
Blood vessels

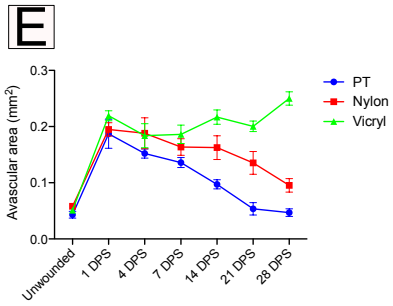
E
Avascular area (mm²)
0.3
0.2
0.1
0.0
Unwounded
1 DPS
4 DPS
7 DPS
14 DPS
21 DPS
28 DPS
PT
Nylon
Vicryl

Figure 5

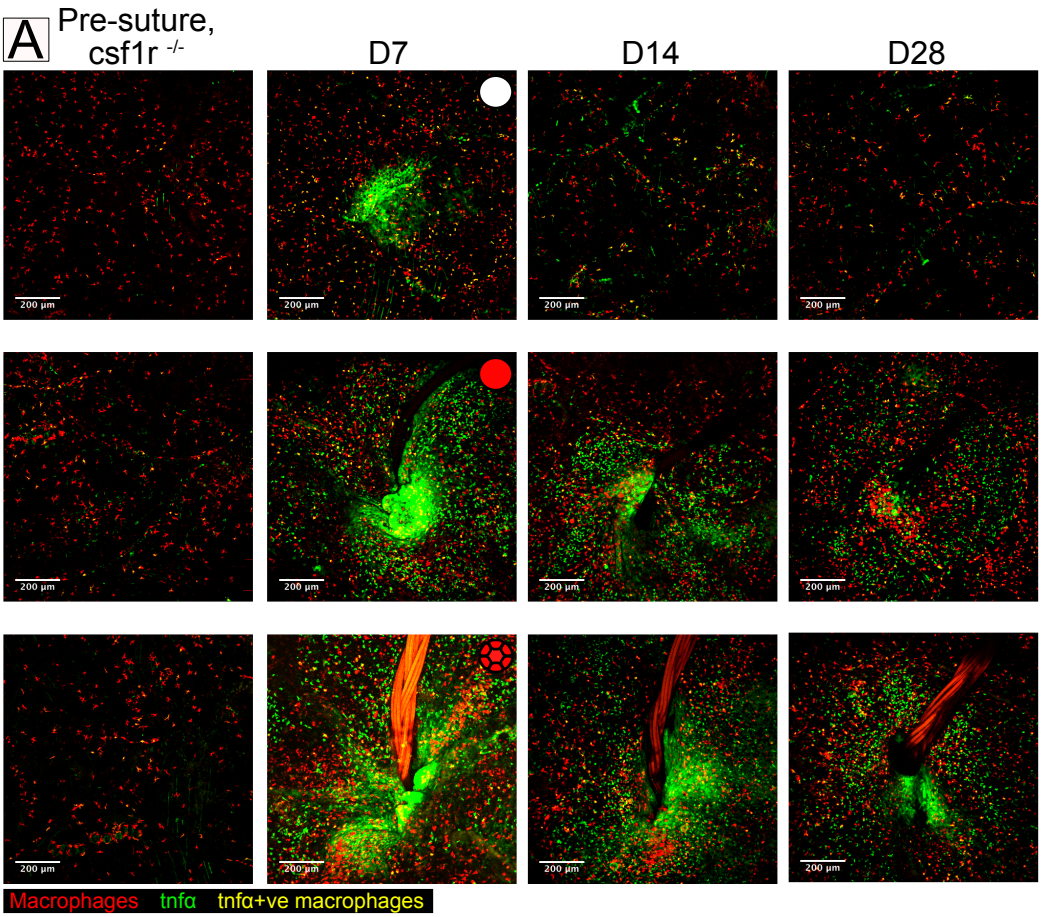
A
Pre-suture, csf1r -/-
D7
D14
D28
200 µm
Macrophages
tnfα
tnfα+ve macrophages

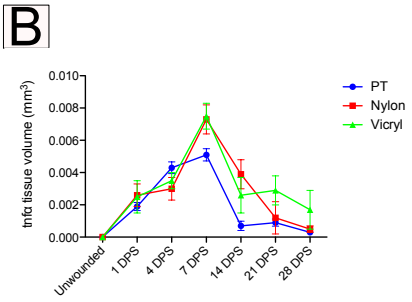
B
tnfα tissue volume (mm³)
0.010
0.008
0.006
0.004
0.002
0.000
Unwounded
1 DPS
4 DPS
7 DPS
14 DPS
21 DPS
28 DPS
PT
Nylon
Vicryl

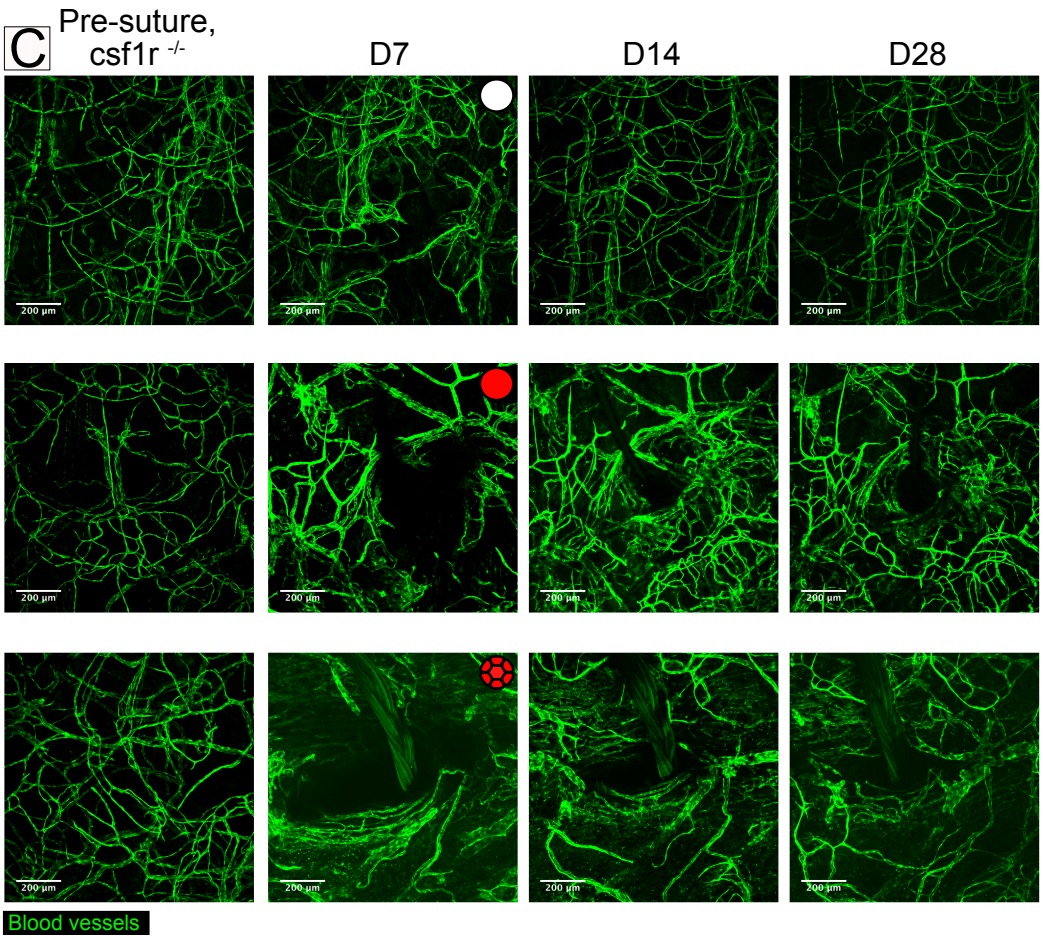
C
Pre-suture, csf1r -/-
D7
D14
D28
200 µm
Blood vessels

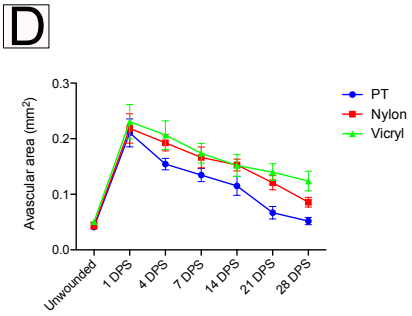
D
Avascular area (mm²)
0.3
0.2
0.1
0.0
Unwounded
1 DPS
4 DPS
7 DPS
14 DPS
21 DPS
28 DPS
PT
Nylon
Vicryl

Figure 6

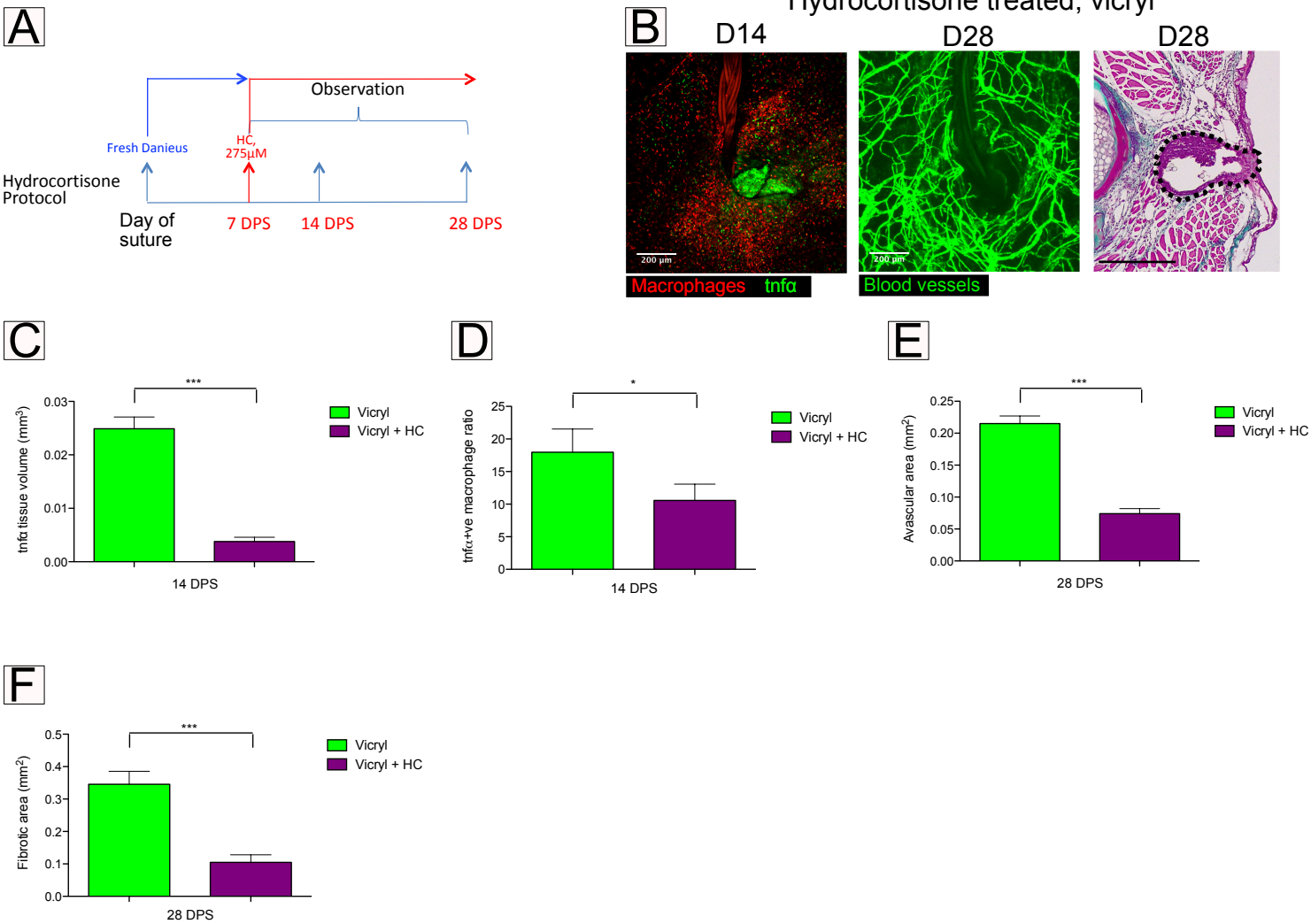
A
Observation
Fresh Danieus
HC, 275µM
Hydrocortisone Protocol
Day of suture
7 DPS
14 DPS
28 DPS
B
Hydrocortisone treated, vicryl
D14
D28
D28
200 µm
Macrophages tnfα
Blood vessels
C
tnfα tissue volume (mm³)
0.03
0.02
0.01
0.00
***
14 DPS
Vicryl
Vicryl + HC
D
tnfα+ve macrophage ratio
25
20
15
10
5
0
*
14 DPS
Vicryl
Vicryl + HC
E
Avascular area (mm²)
0.25
0.20
0.15
0.10
0.05
0.00
***
28 DPS
Vicryl
Vicryl + HC

F
Fibrotic area (mm²)
0.5
0.4
0.3
0.2
0.1
0.0
***
28 DPS
Vicryl
Vicryl + HC